A new mathematical model for irradiance field prediction of upper-room ultraviolet germicidal systems

C.L. Wu [a,b], Y. Yang [a,b], S.L. Wong [b], A.C.K. Lai [b,*]

[a] *Engineering College, Guangdong Ocean University, Zhanjiang 524088, PR China*
[b] *Department of Building & Construction, City University of Hong Kong, Tat Chee Avenue, Kowloon, Hong Kong*

ARTICLE INFO

ABSTRACT

There has been an increasing interest in the use of upper-room ultraviolet germicidal irradiation (UVGI) system because of its proven disinfection effect for airborne microorganisms. To better design and explore further potential applications of UVGI systems, it is of critical importance to predict the spatial UV intensity in enclosures. In this paper, we developed a new mathematical model to predict spatial radiation intensity for upper-room ultraviolet germicidal irradiation systems. The detail geometries of the lamp and the reflector were removed and replaced by introducing a fictitious irradiation surface near louver slots. The view factor approach was applied to evaluate the UV irradiance in a three-dimensional space with different louver configurations. With this approach no detail meshing of the fixture is required and this leads to significant simplification of the entire systems from modeling perspectives.

To validate the model, experiments were performed in a full-scale environmental controlled chamber in which one UVGI fixture was mounted on a sidewall. The UV irradiance was measured by a radiometer. The results predicted by the present model agree very well with the experimental measurements. Factors affect the accuracy of the model was also discussed.

1. Introduction

During the last two decades, aerosols transport and dispersion in indoor environments have caused wide public concerns. Controlling and reducing of human-to-human airborne transmission of contagious pathogens, in particular SARS, tuberculosis, the fatal avian and swine influenza virus is an interdisciplinary issue [1–6]. Interest has grown significantly in the use of ultraviolet germicidal irradiation (UVGI) to disinfect indoor pathogens. The first laboratory studies on using UVGI to sterilize air in surgical operating room dated back to the 1930s [7,8].

One practical application of this concept to disinfect airborne microbes is the use of upper room UVGI installations [9,10]. The advantages of using upper-room UVGI installations in disinfection room include low initial and running costs, less maintenance and easy relocation. It can be installed simply for new and retrofit projects. Currently, upper-room UVGI is recommended by the Centers for Disease Control and Prevention (CDC) as a supplemental approach for preventing transmission of tuberculosis in isolation rooms [11] and has been applied in shelters for homeless [12]. Human exposure to UVC should be minimized as excessive expo-

sure causes eye or skin irritation. Recommended dose limits for occupations is below 6 mJ for 8 h [13]. With this potential health threat, one successful application of UVGI is to irradiate the upper part of a room while minimizing radiation exposure of persons at the lower part of the room to avoid overdose by skin and eyes. Thus bare lamps can never be used in practical installations. Instead, UVGI fixtures with inclined multi-louvers are normally used to generate collimated, parallel rays irradiating to the upper-zone of rooms in order to shield the UV rays from being directly viewed by occupants. A reflector is normally installed behind the lamp to maximize the output.

The performance of any UV devices against a particular airborne microorganism can be generally described in terms of the fraction of microorganisms surviving following irradiation, given by [14]:

$$C(t) = C_0 e^{-ZE_p t} \qquad (1)$$

where C_0 is the initial microorganism concentration (cfu m^{-3}), Z is the susceptibility constant of the microorganisms to the irradiation for a given microorganism (m^2/J), E_p is the irradiation intensity (W/m^2) and $C(t)$ is the concentration at time t (s) following UV irradiation (cfu m^{-3}).

The irradiation intensity, E_p, is a controlling parameter influencing the UVGI system efficacy. The intensity distribution is a function of spatial position relative to the lamp fixture, and it depends on a few important parameters such as the lamp configuration, wall
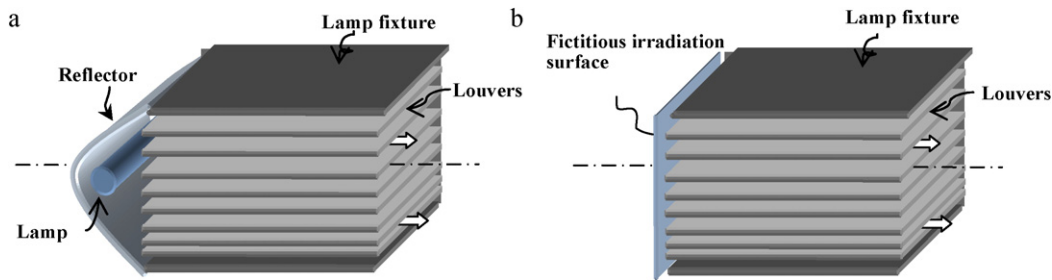
Fig. 1. Introduction of the fictitious surface: (a) the schematic of multi-louvered UV fixture and (b) simplification of the UV lamp by an equivalent UV irradiation plane.
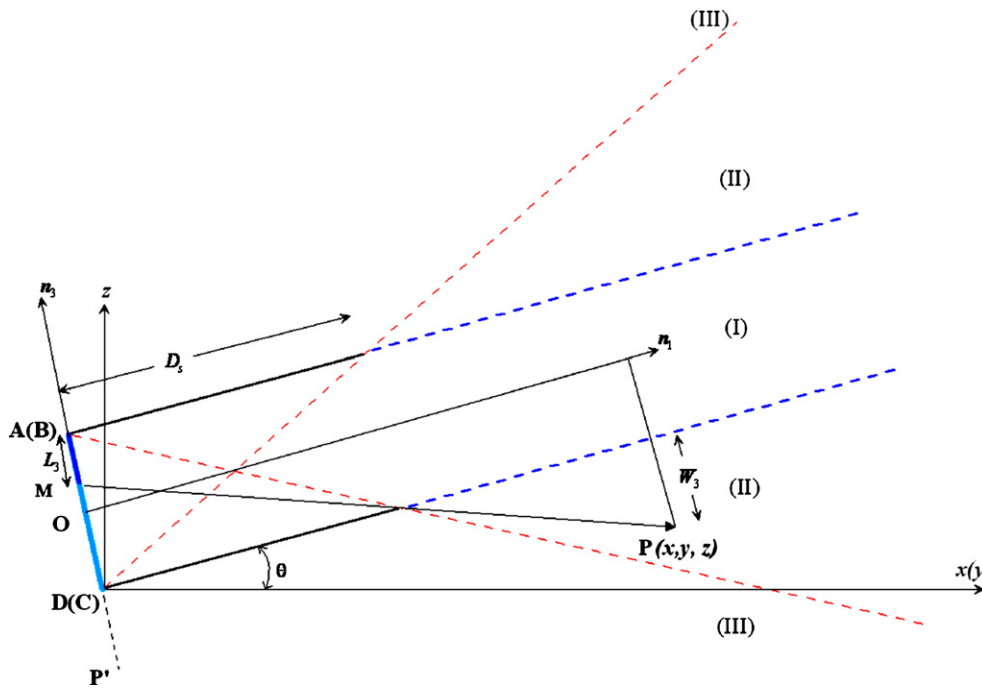

Fig. 2. Illustration of the calculation of the view factor between sub-surface ABCD and the observation point *P*.

reflectance, air relative humidity and temperature and room configuration in which some of them have been discussed previously [15,16]. The dose received by the microorganisms depends on the above factors affecting E_p and the (vertical) air movement entering-and-leaving the irradiated zone. The efficacy of the upper-room UVGI has been measured and reported in a number of studies [15,17–20]. In fact current understanding on system installation was acquired by trial-and-error methods and translated into rules of thumb [21,22].

Mathematical approaches such as analytical and computational have been applied and reported in the literatures. Under the analytical approach, a room was divided into two zones; a lower, irradiant-free zone and an upper, irradiated zone [23–25] or even three zones [26,27]. Systems of equations were solved to evaluate the zonal concentration. Though the simplicity, the approach did not take into account the variation of room air velocities across the room, and most importantly uniform irradiance field in the upper-zone was assumed. Computational approach is needed to model the efficacy of a unique UVGI system and an exclusive set of operation conditions. Conventionally the approach consists of two sequential steps; first computing the UV field and followed by evaluating the concentration of microorganisms by computational fluid dynamics analysis. This paper focuses on the first step.

Two methodologies for modeling UV intensity field have been proposed, named the inverse square law [14,28] and the view factor approach [29,30]. However, these models are limited to applica-

tions of bare UV lamps, while the lamp reflector, the fixture and the louvers have not been included. These simplifications lead the models that cannot be applied for real-life upper-room UVGI systems. Due to the complicated geometry of the real UV lamp configuration, it is difficult to predict the UV intensity distribution analytically. Recently, the effects of lamp radius and sleeve on radiation field around a UV lamp were reported for water disinfection [31]. For indoor application, one study developed a mathematical model to predict UV irradiation level for upper part of a room [32]. Nevertheless the model was only valid for pendant-type fixtures.

In this work, we developed a novel yet simple mathematical model with the view factor method to predict spatial UV intensity for indoor environments installed with multi-louvered wall-mounted UV fixtures. The model was validated through a comprehensive comparison of the modeling results with experimental measurements conducted in a full-size environmental chamber.

2. Mathematical model

The core model for predicting lamp intensity and the reflected component of radiation is based on radiation view factors [33]. The intensity of the UV radiation from the specific fixture depends not only on the lamp power output, but also on the fraction of this output that exits the fixture or the louvers. An example of multi-louvered fixture is shown in Fig. 1(a). The three-dimensional meshing of the complicated geometry in Fig. 1(a) makes it very

Table 1
Parameters of modeling cases.

	E_s (W)	H_{uv} (m)[a]	L_s (m)	H_s (m)	D_s (m)	N_s	θ_L[b]
Case 1	5.3	2.05	0.27	$0.11/N_s$	0.0	1	0°
Case 2	5.3	2.05	0.27	$0.11/N_s$	0.14	14	0°
Case 3	5.3	2.05	0.27	$0.11/N_s$	0.14	14	5°

[a] The height of UV lamp center.
[b] The inclined angle of the louver.

difficult or almost impossible to predict spatial UV intensity straightforwardly. To simplify the calculation, we introduced a fictitious surface near the louver inlet slots to represent the UV lamp (see Fig. 1(b)). The finite-size cross section at the internal side of the fixture is served as an equivalent UV irradiance surface. This fictitious source irradiates UV lights with a UV output approximately the same as the lamp output power. The simplification is justified by the fact that both the lamp and the reflector are very close to the louver slots, and the reflector casts almost all UV rays passing through the internal cross section of the fixture. At this stage, we assumed that the fraction output of the UV lamp entering this fictitious surface is f, which can be adjusted with the reflector actual condition. Thus, the equivalent UV output from this fictitious surface is

$$E_s = fE_{uv} \tag{2}$$

where E_{uv} is the UV power output of lamp.

A well-designed reflector arch can distribute the radiation very uniformly to the louver slots. In such a case, the UV emission intensity at the whole fictitious surface can be deemed as uniform and
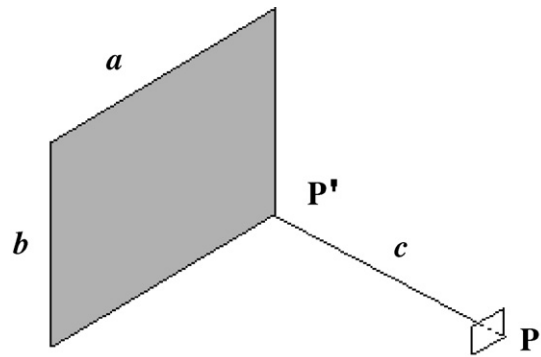

Fig. 3. Calculation of the view factor between a differential surface and a finite surface.

is calculated by

$$I_s = \frac{E_s}{A_s} \tag{3}$$

where $A_s = N_s H_s L_s$ is the total area of the slot cross section, L_s is the slot length, H_s is the slot height and N_s is the number of louver slots. For the case of a heterogeneous distribution of the surface UV output, we have

$$E_s = \int_A I_s(x,z)\,dxdz \approx \sum_{i=1}^{N_s} I_{s,i} H_{s,i} L_{s,i} = H_s L_s \sum_{i=1}^{N_s} I_{s,i} \tag{4}$$
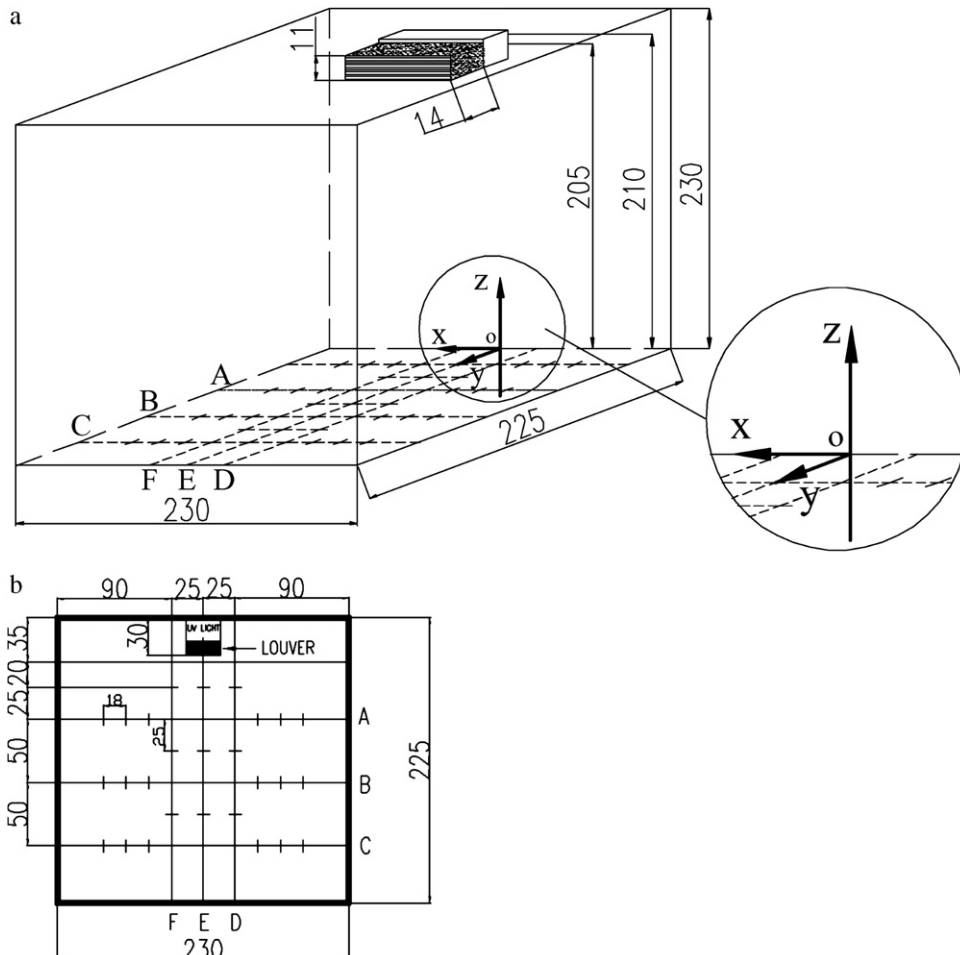

Fig. 4. Configurations of experiment room: (a) schematic of the fixture and (b) arrangement of the measured points. All dimensions are in cm.
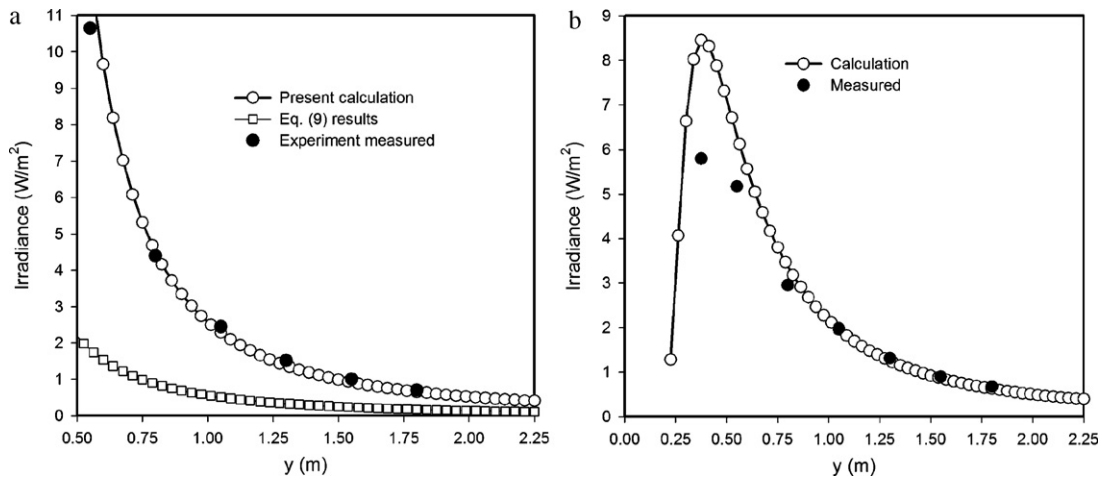
Fig. 5. UV irradiance distribution in y direction with no louver case (Case 1) at $z = 2.05$ m. (a) Present model results compared with those predicted by a bare lamp (Eq. (9)) at E–E and (b) D–D.
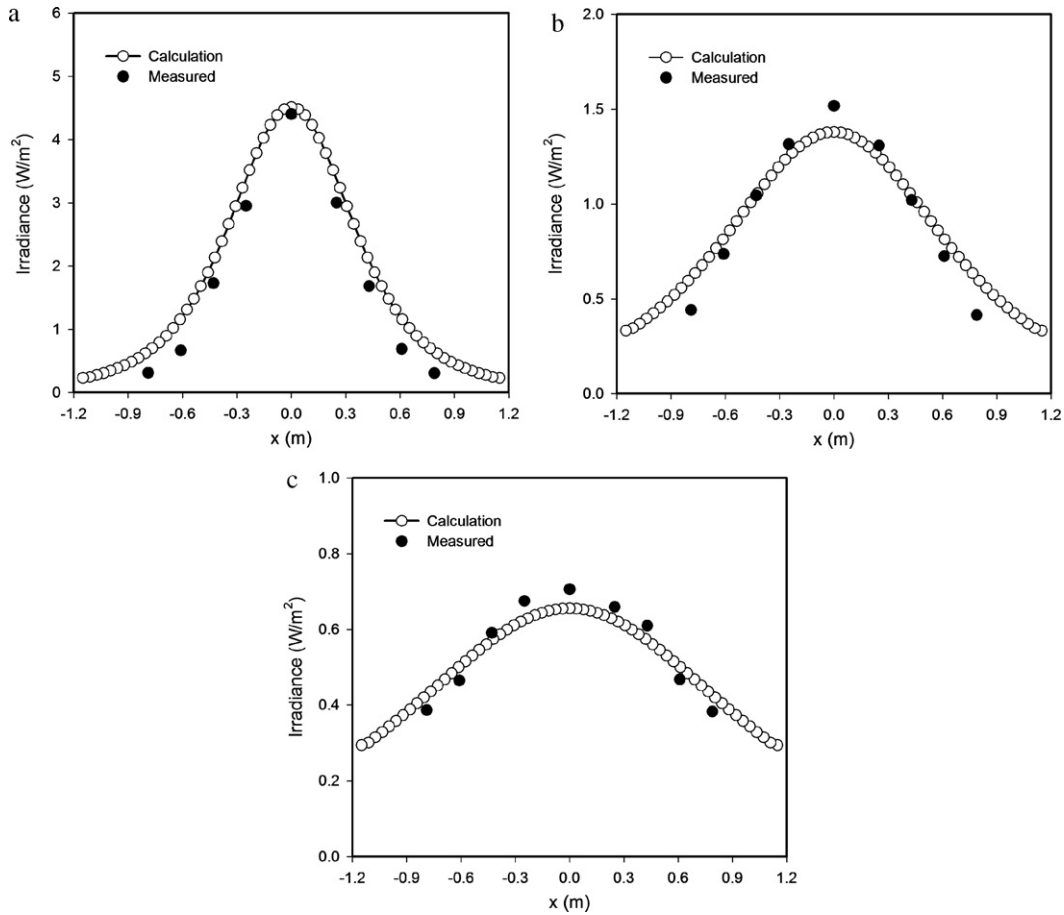

Fig. 6. UV irradiance distribution in x direction with no louver case (Case 1) at $z = 2.05$ m: (a) A–A, (b) B–B and (c) C–C.

with the assumption that all the louver slots have the same dimensions. $I_{s,i}$ is the UV output intensity of the fictitious sub-surface corresponding to the ith slot.

Through the introduction of the fictitious irradiation source, the UV intensity $I(x, y, z)$, for a given differential surface at the observation point $P(x, y, z)$, can be calculated by the summation of the view factors between the surface and the all slot sub-surfaces:

$$I = \sum_{i=1}^{N_s} I_{s,i} F_{d1-i}$$ (5)

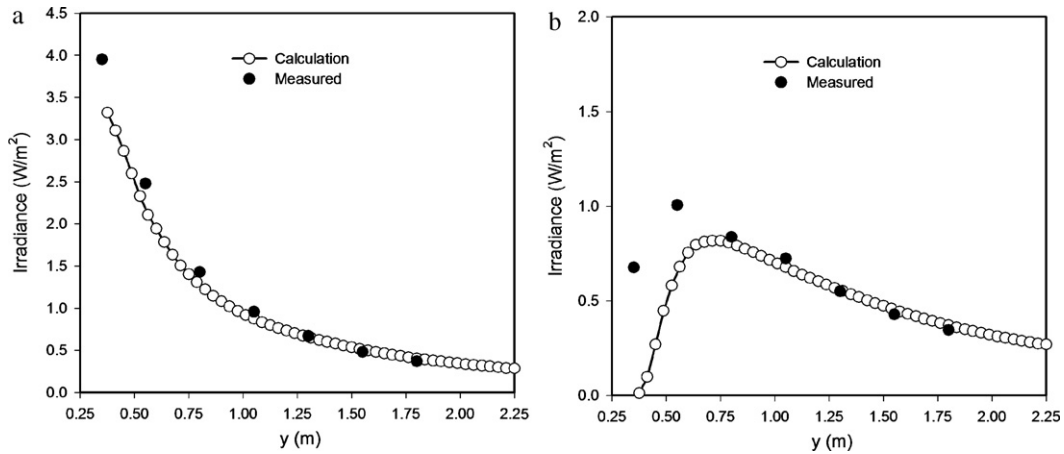where F_{d1-i} is the fraction of thermal power leaving differential surface 1 and reaching the ith slot.

Fig. 7. UV irradiance distribution in y direction with horizontal louver (Case 2) at $z = 2.05$ m: (a) E–E and (b) D–D.
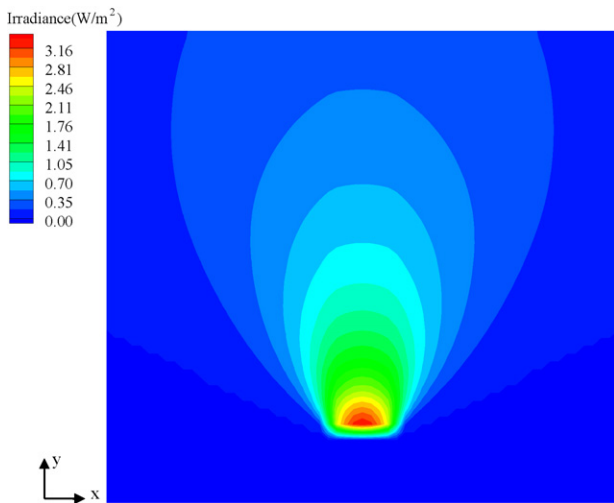

Fig. 8. The UV irradiance contour field with horizontal louver surface (Case 2) at $z = 2.05$ m.

Fig. 2 illustrates the calculation of the view factor for a sub-surface i corresponding to a given slot. Three zones in space are distinguished depending on the range in which the sub-surface can be seen at the point $P(x, y, z)$ through the louver slot. We defined a local coordinate $O\text{-}\mathbf{n}_1\mathbf{n}_2\mathbf{n}_3$ with the origin placed at the center of the sub-surface $O (x_i, y_i, z_i)$. The unit normal vector of the sub-surface is $\mathbf{n}_1$ and the unit vector along the lamp axis is $\mathbf{n}_2$. We suppose the dimensions of the surface area border seen from the observation point P in $\mathbf{n}_3$ and $\mathbf{n}_2$ is L_3 and L_2, respectively. The depth and length of the louver slot are D_s and L_s, respectively. Other parameters are denoted in Fig. 2. Obviously, if P is in region III, the observer cannot receive the UV radiation from this slot and we have $L_3 = 0$; if P is in region II, the observer can receive part of UV radiation from the slot, and we have $0 < L_3 < H_s$, while $L_3 = H_s$ as P in region I and the full radiation from the slot can be received by the observer. L_3 can be determined via some geometry relations:

$$
L_3 = \begin{cases}
H_s & \text{if } W_3 \leq 0 \quad (P \text{ is in region I}) \\[1em]
H_s - \dfrac{W_3 D_s}{W_1 - D_s} & \text{if } W_3 > 0 \text{ and } H_s > \dfrac{W_3 D_s}{W_1 - D_s} \\
\quad (P \text{ is in region II}) & \\[1em]
0 & \text{if } W_3 > 0 \text{ and } H_s \leq \dfrac{W_3 D_s}{W_1 - D_s} \\
\quad (P \text{ is in region III}) &
\end{cases}
\tag{6}
$$

where $W_3 = |\mathbf{PO} \cdot \mathbf{n}_3| - (1/2)H_s$, and $W_1 = |\mathbf{PO} \cdot \mathbf{n}_1|$

Similar formulas can be obtained and used to calculate the sub-surface dimension L_2 in $\mathbf{n}_2$-direction that can be seen from the observation point:

$$
L_2 = \begin{cases}
L_s & \text{if } W_2 \leq 0 \\[1em]
L_s - \dfrac{W_2 D_s}{W_1 - D_s} & \text{if } W_2 > 0 \text{ and } L_s > \dfrac{W_2 D_s}{W_1 - D_s} \\[1em]
0 & \text{if } W_2 > 0 \text{ and } L_s \leq \dfrac{W_2 D_s}{W_1 - D_s}
\end{cases}
\tag{7}
$$

where $W_2 = |\mathbf{PO} \cdot \mathbf{n}_2| - (1/2)L_s$.

Once the valid UV irradiation source of the sub-surface is determined, as shown in Fig. 3, the view factor for the differential area can be calculated through some algebraic operations of the following formula:

$$
F_{d1-f} = \frac{A}{2\pi(1+A^2)^{1/2}} \tan^{-1}\left[\frac{B}{(1+A^2)^{1/2}}\right] + \frac{B}{2\pi(1+B^2)^{1/2}} \tan^{-1}\left[\frac{A}{(1+B^2)^{1/2}}\right]
\tag{8}
$$

where $A = a/c$ and $B = b/c$. The above formula gives the view factor of a differential planar element placed at a distance c from the corner of a finite parallel rectangle with a width a and height b [33]. Referring to the above calculations, we have $c = W_1$. The algebraic operation of the above formula depends on the region in which the Point P falls in the vertical and axial directions, respectively. The details are shown in Appendix A.

Given the fixture axial direction $\mathbf{n}_2$ and the louver inclined angle θ or the slot normal direction $\mathbf{n}_1$, the visible dimensions of one fictitious surface from any space point will be determined through Eqs. (6) and (7). Then the view factor can be calculated with Eq. (8). Finally, the UV irradiation intensity at any point in space can be obtained with Eq. (5).

3. Model validation

3.1. Experiment set-up

The experiments were conducted in an environment-controlled room with dimensions 2.25 m (L) × 2.3 m (W) × 2.3 m (H). The walls are insulated by fiberglass. There is one door and no windows. Since no bio-aerosols were used at this stage, no ventilation was provided during the measurement. To facilitate model validation, it is important to keep the parameters to a minimum. To eliminate internal surface reflection, all the surfaces including the diffusers were covered by black papers. One side-wall UVC germicidal fixture
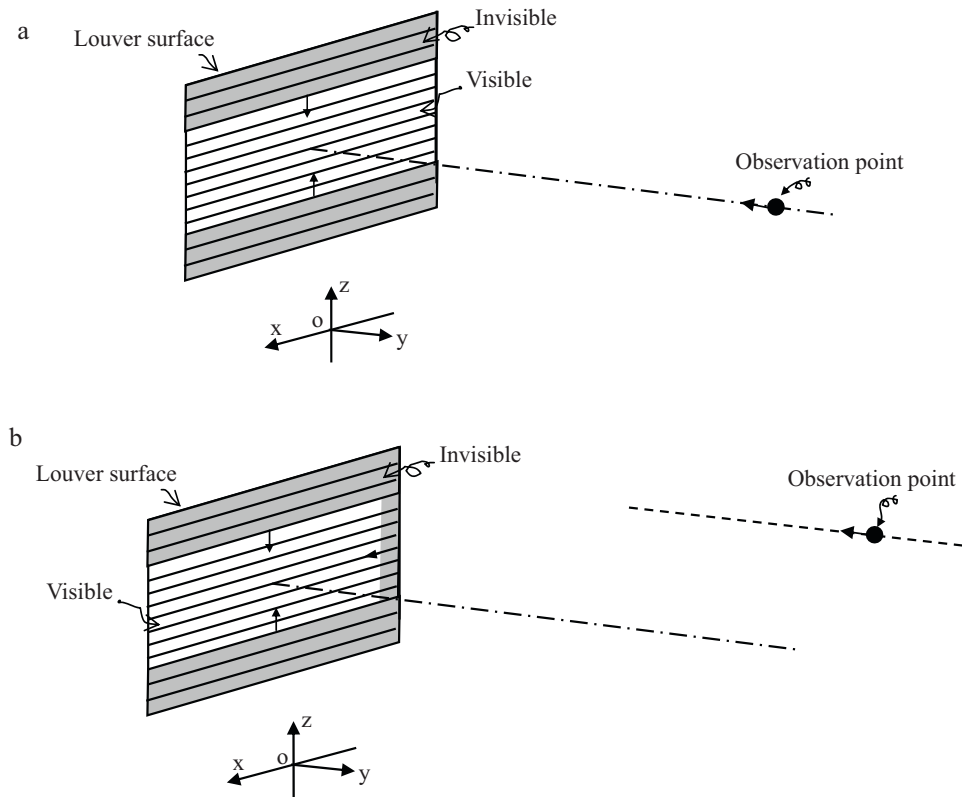
Fig. 9. Schematic diagram of the fixture shielded effect: (a) observation point located at the center line of the fixture and (b) observation point located to the side of the fixture.

(TB-12-W, American Ultraviolet) was mounted along the center of the wall. The UVC fixture holds a UVC lamp of 16 W.

The intensity was measured by a radiometer (IL1400, International Light Technologies) equipped with a suitable detector with a peak at 254 nm (SEL/NS254/W). The meter and the sensor were brand new and have been factory-calibrated before shipping. The sensor was mounted on a tripod. As the intensity is very sensitive to the source orientation, particularly at the vicinity of the fixture, it is very crucial to ensure that the detector faces perpendicularly to the fixture.

The intensity was measured at two horizontal heights, namely 205 cm and 210 cm. All the measurement points were marked on the floor to facilitate accurate location measurement and they were shown in Fig. 4.

Prior to the measurement, the lamp was turned on for 30 min. Each point measurement was repeated at least three times. One particular observation to check for the quality of the data is their symmetry along the central line. For instances if the data for points A and B are similar, the reliability of both data would be high otherwise measurements were repeated.

The lamp reflector used in our experiment is made of smooth, thin stainless steel covered with polished aluminum foil and hence we assumed the value was 1.0. The effect of wall reflection was ignored here. Conventionally it can be measured with spherical actinometry method [34,35]. In actual condition, the reflectivity of wall for 254-nm ultraviolet radiation mainly depends on the wall material surface [25,32,36]. For most of painted walls, the reflection for 254-nm ultraviolet radiation is on the order of 5% [32].

3.2. Model validation

The mathematical model developed in the present work was applied to study the irradiance field with identical dimensions those of the experimental chamber. To compute the UV intensity at space, the closure was meshed by $60 \times 60 \times 60$ grids. The fictitious surface was located between the UV lamp and the louver fixture ($y = 0.2$ m). The other modeling parameters are summarized in Table 1.

4. Results and discussion

4.1. Case 1: no louver

In the experimental set-up, the louver of the fixture was removed while keeping the lamp holder box and the reflector. To match the experiment conditions, the louver depth was set zero in our numerical model. Likewise, the comparison of our model and the existing bare lamp model was also discussed. In reported bare lamp model, the spatial radiance is calculated as [30,36]:

$$I = \frac{E_s}{2\pi r l} F_{d1-2} \tag{9}$$

where r is the radius of the lamp, l is the length of the lamp, and F_{d1-2} is the fraction of radiative intensity leaving differential surface 1 and reaching UV lamp. It can be obtained with [33]:

$$F_{d1-2} = \frac{1}{\pi H} \tan^{-1} \frac{L}{\sqrt{H^2 - 1}}$$

$$+ \frac{L}{\pi} \left[\frac{X - 2H}{H\sqrt{XY}} \tan^{-1} \sqrt{\frac{X(H-1)}{Y(H+1)}} - \frac{1}{H} \tan^{-1} \sqrt{\frac{H-1}{H+1}} \right] \tag{10}$$

The parameters in Eq. (10) are defined as follows:

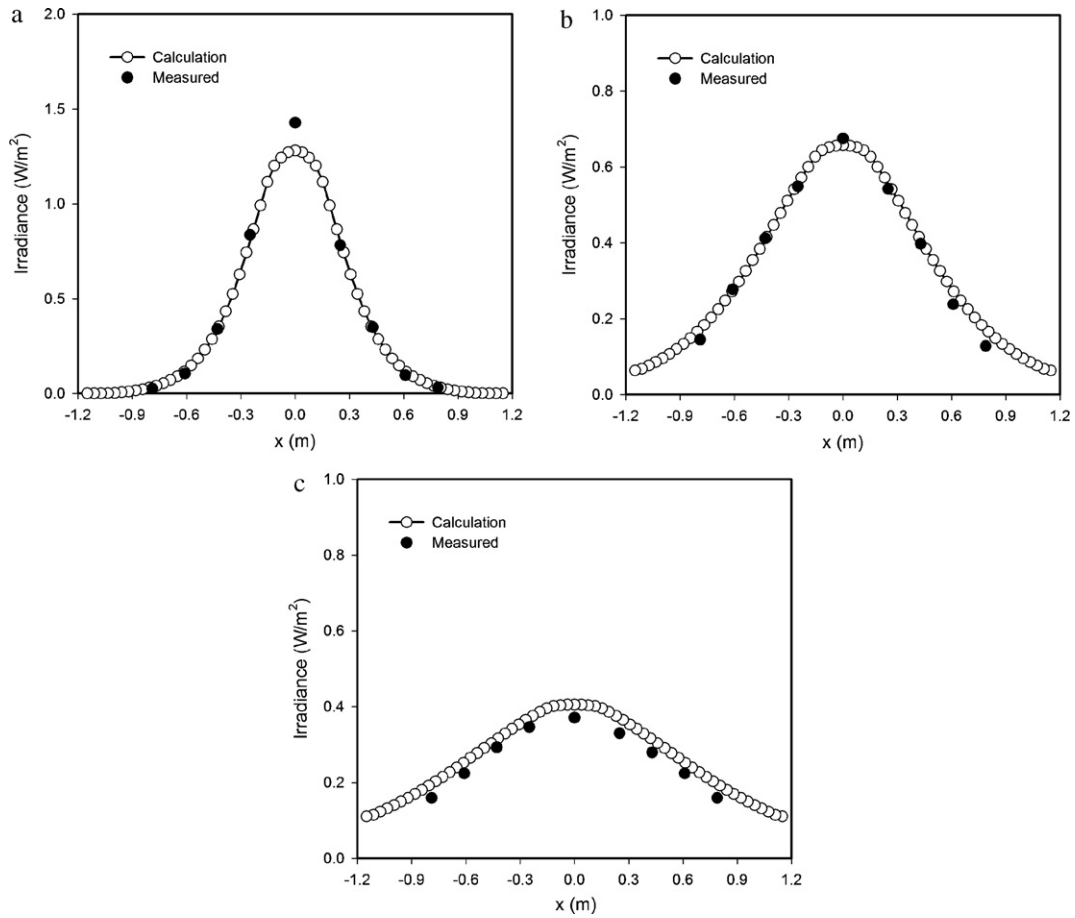$$L = \frac{l}{r}, \quad H = \frac{h}{r}, \quad X = (1+H)^2 + L^2, \quad Y = (1-H)^2 + L^2$$

Fig. 10. UV irradiance distribution with horizontal louver (Case 2) at $z = 2.05$m: (a) A–A, (b) B–B and (c) C–C.

where h is the distance between the differential surface and the lamp. If differential surface 1 is not at the end of the cylinder, F_{d1-2} is calculated with algebraic operation.

Fig. 5 shows the radiation intensity along E–E and D–D at $z = 2.05$ m, respectively. It can be seen that the bare lamp model under-predicts the UV intensity considerably and the irradiances read less than 25% of the experimental measurements. This substantial discrepancy is incurred by the negligence of the reflector, which reflects almost all the UV rays. However, in the present model, the reflection effect is taken into account by assuming an equivalent UV output of the fictitious source to that of the lamp. This consideration improves the modeling accuracy greatly. Fig. 5(b) shows that the present model predicts UV intensity approximately 20% higher than the measurement where the observation point is very close to the fixture (D–D). This discrepancy is attributed to the ignorance of the lamp fixture shading effect on UV source distribution. That is to say that uniform UV source distribution in fictitious surface is not an ideal way. The corresponding discussion on this point is presented at Section 4.4. The axial profiles of the UV intensity at three distances from the fixture are also compared to the experimental measurements, as shown in Fig. 6. One characteristic of the radiation intensity distributions is that the profile becomes much flatter as the distance from the fixture increases. The peak value of the radiation intensity always occurs at the center of the fixture.

4.2. Case 2: horizontal louver

In this case the louver slices were added and configured horizontally. A comparison of the prediction and experiment along E–E

and D–D at $z = 2.05$ m is shown in Fig. 7. It can be seen that the radiation intensity decreases monotonously as the observer departs from the fixture along E–E, while it increases to a peak value of about 1 W/m² and then decreases gradually as the observer departs from the left sideward of the fixture along D–D. These two profiles of the radiation intensity are also confirmed from the "growing-bubble" contours of the intensity field at the horizontal plane at $z = 2.05$ m, as shown in Fig. 8. The difference is partly attributed to the shielding effect of the fixture sidewall. The radiation intensity calculated by the view factor equation (Eq. (8)) diminishes more rapidly at the location close to the source surface than that at the location far from it. It is easy to prove that

$$\delta F_{d1-f} = \frac{\partial F_{d1-f}}{\partial A}\left[\frac{1}{c}\left(\delta a + \delta b - \frac{(a+b)\delta c}{c}\right)\right] \qquad (11)$$

with $(\partial F_{d1-f}/\partial A) = (\partial F_{d1-f}/\partial B) > 0$.

If the fictitious surface is fully visible and $a = a_0$, $b = b_0$, Eq. (11) reads as

$$\delta F_{d1-f}^{(0)} = \frac{\partial F_{d1-f}}{\partial A}\left[-\frac{(a_0+b_0)}{c^2}\delta c\right] \qquad (12)$$

and given $0 < c_1 < c_2$, one obtains $(|\partial F_{d1-f}/\partial c|_{c=c_1}) > (|\partial F_{d1-f}/\partial c|_{c=c_2})$. where a and b are the width and height of the visible surface, respectively, and c is the normal distance from the observer to the source surface, as defined in Fig. 3.

It can be imagined that the observer approaches to the UV fixture from locations far away by two trajectories, with one aligned to the fixture center (E–E) and the other aligned to the lateral side at a distance of 0.25 m from the fixture center (D–D), at the horizontal plane $z = 2.05$ m. In the former case, all the sub-surfaces are
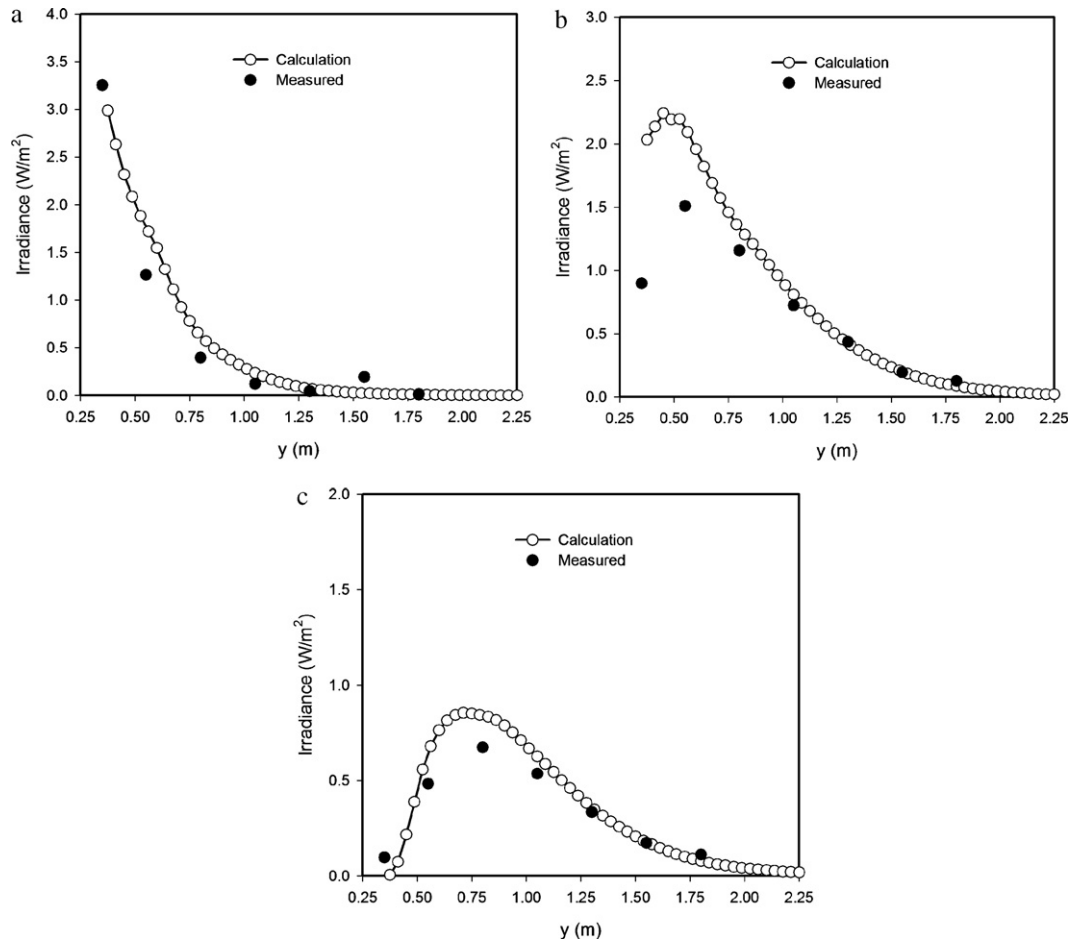
Fig. 11. UV irradiance distribution with 5 angle inclined louver (Case 3): (a) E–E at $z = 2.05$ m, (b) E–E at $z = 2.1$ m and (c) D–D at $z = 2.1$ m.

visible to the observer at the beginning, thus the radiation intensity increases due to the decrease of the distance from the UV source ($\delta c < 0$). Then, when the observer moves towards the fixture, the louver grids at the top and the bottom of the fixture begin to shield the UV rays and the total visible area of the sub-surfaces decreases ($\delta b < 0$ and $\delta a = 0$). Since the shielded surfaces locate at the top or bottom of the fixture, they are always much further away from the observer, which is at the center of the fixture, comparing to the visible sub-surfaces, as shown in Fig. 9(a). Moreover, there are two sub-surfaces (the central ones) fully visible from the observer (we have ignored the thickness of the louver slice). The increasing proportion of the radiation from the visible sub-surfaces due to the decrease of distance is much larger than the reducing radiation from other sub-surfaces due to the decrease of visible areas. From geometric relations, we have

$$b = \frac{2H_s(c - D_s)}{D_s} \tag{13a}$$

$$\delta b = \frac{2H_s}{D_s}\delta c \tag{13b}$$

To substitute Eq. (13) into Eq. (11), the expression of Eq. (11) can be rewritten as

$$\delta F_{d1-f}^{(1)} = \frac{\partial F_{d1-f}}{\partial A}\frac{2H_s - a_0}{c^2}\delta c \tag{14}$$

Compared to Eq. (12), Eq. (14) also can be described as

$$\delta F_{d1-f}^{(1)} = \delta F_{d1-f}^{(0)} + \delta F'_{d1-f} \tag{15}$$

with $\delta F'_{d1-f} = (\partial F_{d1-f}/\partial A)(2H_s + b_0/c^2)\delta c$

Since the single louver height H_s is much smaller than the louver width L_s ($\delta a = 0$, so $a = L_s$ is a constant), we always have $\delta F_{d1-f}^{(1)} > 0$ with $\delta c < 0$. Therefore, a monotonously intensified radiation profile is observed, as shown in Fig. 7(a). $\delta F'_{d1-f}$ can also be considered as the fraction of radiation shielded by louvers. This part becomes significant when the observer is close to the lamp, resulting in a much less radiation increase near the lamp when comparing to that in at no louver configuration (see Fig. 5(a)).

In the latter case, similar trend occurs when the observer receives almost all the coverage of the sub-surfaces. When the distance decreases gradually, one of the fixture sidewalls begins to shield some UV rays besides the top and bottom louvers ($\delta b < 0$, and $\delta a < 0$), as shown in Fig. 9(b). At the beginning, the proportion of the increased UV intensity due to decreasing of distance from the UV source is much larger than the decreasing proportion by the shielding effect of both the sidewall and the louver slices, which results in a general increase of the irradiance. The shielding lateral dimension of the sidewall can be calculated similarly to Eq. (13):

$$a = a_0 - \frac{D_s L_p}{(c - D_s)} \tag{16a}$$

$$\delta a = \frac{D_s L_p}{(c - D_s)^2}\delta c \tag{16b}$$

Using Eq. (13) and Eq. (16), Eq. (11) can be expressed as

$$\delta F_{d1-f}^{(2)} = \frac{\partial F_{d1-f}}{\partial A}\left[\frac{2H_s - a_0}{c^2} + \frac{D_s L_p(2c - D_s)}{c^2(c - D_s)^2}\right]\delta c \tag{17}$$
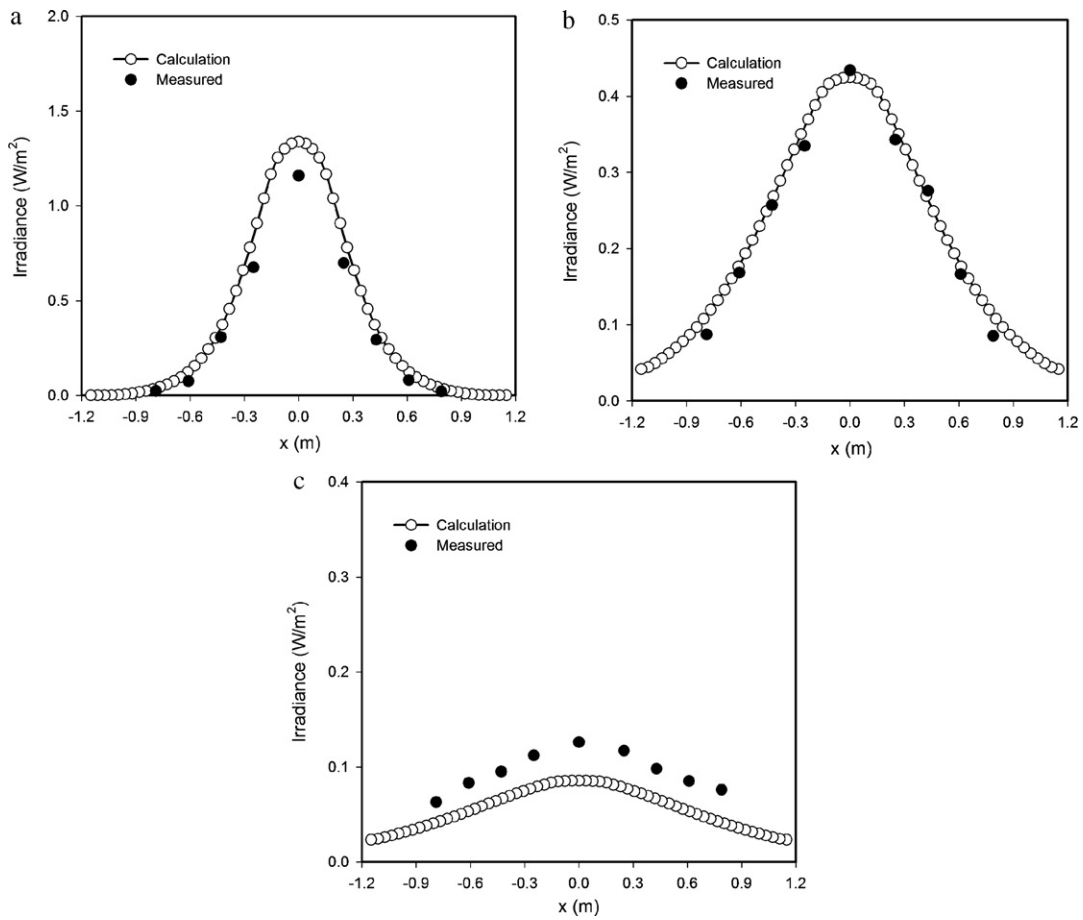
Fig. 12. UV irradiance distribution in x direction with 5° louver (Case 3) at $z = 2.1$ m: (a) A–A, (b) B–B and (c) C–C.

Compared to Eq. (12), Eq. (17) also can be expressed as

$$\delta F_{d1-f}^{(2)} = \delta F_{d1-f}^{(0)} + \delta F_{d1-f}' + \delta F_{d1-f}'' \tag{18}$$

where $\delta F_{d1-f}' = (\partial F_{d1-f}/\partial A)(D_s L_p (2c - D_s)/c^2 (c - D_s)^2)\delta c$, and $L_p = 0.25 - 0.5 a_0 \approx 0.5 a_0$ is the lateral distance from the observer to the fixture side wall.

$\delta F_{d1-f}''$ can be considered as the proportion of radiation shielded from the fixture side wall. It becomes significant if the lateral distance L_p is large or/and the depth of the fixture is large while the observer is close to the lamp. If $c > 2.36 D_s$, Eq. (17) yields $\delta F_{d1-f}^{(2)} = (\partial F_{d1-f}/\partial A)\lfloor -(0.5 a_0 (2c^2 - 6 D_s c + 3 D_s^2)/c^2 (c - D_s)^2)\delta c\rfloor > 0$.
Herein, we assume $2 H_s - a_0 \approx -a_0$ and $L_p \approx 0.5 a_0$ since $H_s \ll a_0$. This means that irradiance increases as the observer distance c decreases to approximately twice the louver depth D_s. Since both dimensions (a and b) of the visible source surface decrease as the observer approaches the fixture and a decrease of the view factor will occur: $\delta F_{d1-f} < 0$ if $c < 2.36 D_s$. Given the initial parameters, the peak value of the view factor should occur at $y = 0.53$ m ($c = 0.33$ m). The above analysis is based on Eq. (8) assuming that the observer is always aligned to the corner of the visible surface, however it is not the practical situation. In reality the shielded surface with increasing dimensions is much closer or almost aligned to the observer while the visible surfaces with decreasing dimensions are far away from the observer. This concludes that increasing the area of the ghost surfaces has a dominant and negative contribution to the final view factor. The predicted model of the maximum UV intensity occurs at $y = 0.6$ m, which closes to the experimental result ($y = 0.55$ m). The maximum radiation intensity is about 0.8 W/m² , which is slightly lower than the measured value of

1.0 W/m² . It can be seen that the developed model captured the above two different profiles and the modeling results agree very well with the experimental measurements, as shown in Fig. 7.

The sidewall shielding effect can also be observed from the axial profiles of the radiation intensity, as shown in Fig. 10. It can be seen that the maximum radiation intensity always occurs at the center of the fixture. The profile becomes flatter and its value decreases as the horizontal distance increases. This is because the sidewall can shield less UV rays if the normal distance to the observer is kept farther away from the UV source. It is observed that the profiles are sharper if compared to the no-louver configuration, as shown in Fig. 10(a). This implies that the sidewalls of the UVGI fixture have a significant influence to the distribution of the radiation intensity. Both the predicted and measured irradiances are much lower than those of no-louver configuration since the louver slices shield most of UV rays. It can be concluded that a mathematical model ignoring the fixture and louver dimensions is not applicable to evaluate the efficacy of the upper-room UVGI system with louvers.

4.3. Case 3: 5° inclined louver

Very often the ceiling of rooms restricts the installation height of UVGI fixture. To enhance the maximum efficacy while keeping the exposure below the threshold limit, the louvers are always inclined horizontally at a small angle directing the collimated beams upwards to minimize the human exposure. In this case, the irradiance field for 5° upward inclined louver surface is analyzed, which is identical to the experimental conditions.

Fig. 11 shows UV irradiance distribution in y direction with 5° inclined louver surface. At the horizontal plane aligned with the

center of the lamp ($z = 2.05$ m), the magnitude of the irradiance at the measurement point, which is nearest to the fixture, is almost the same as that in Case 2, but it diminishes quickly as the observer departs from the lamp. It can be noticed that there is almost no irradiation detectable at those locations with a distance more than 1.25 m from the fixture. This suggests that the penetrability of the direct UVC at $z = 2.05$ m plane was weakened by the inclined louver surfaces. The irradiance influence region is actually shifted to the plane at $z = 2.1$ m. However, at the plane $z = 2.1$ m, the shielding effect from the bottom louvers is still very evident while the observation point is close to the fixture. Fig. 11(b) and (c) shows the short-term increase of the UV intensity profiles by the shielding effect. Fig. 12 shows the lateral profiles of the UV irradiance at three distances from the louver in the plane $z = 2.1$ m. It can be seen that the prediction is more precise in near lamp field than in remote region, where the irradiance is close to zero and is under-predicted by the model.

4.4. Effects of reflector

An ideal parabolic reflector made from ideal material can reflect 100% horizontal light ray. In practice, non-ideal situation is encountered. Generally, the reflectivity of polished aluminum reflector ranges from 0.79 to 0.91 [36,37]. In order to investigate the effect of possible reflectivity with our reflector, the additional results of $f = 0.9$ is studied in details.

For all modeling results presented, uniform UVC intensity distribution method was assumed and applied to the model. The fictitious surface length was set equal to the length of the fluorescent tube (0.27 m). To further explore how non-uniform intensity
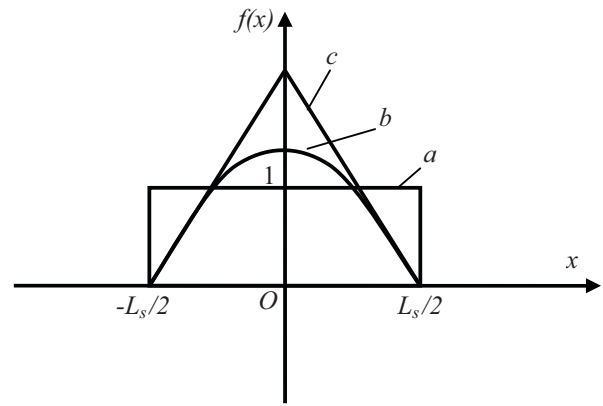

Fig. 13. Different irradiative source intensity distribution methods: (a) uniform, (b) parabolic and (c) linear.

affects the modeling results, Eq. (2) was modified as follows:

$$E_s = f \times f(x) \times E_{uv} \qquad (19)$$

where $f(x)$ is the UVC intensity distribution function along the fictitious surface. As shown in Fig. 13, two additional distribution functions were introduced and both of them have the same integral areas of the uniform distribution. Their mathematical expression is given in Table 2.

Fig. 14 presents the results of horizontal louver case (Case 2) with setting $f(x) = 1.0$ and $f = 1.0$ or 0.9. The modeling results predicted with $f = 1.0$ near the lamp is slightly better than those by $f = 0.9$. The results of different non-uniform source intensity distri-
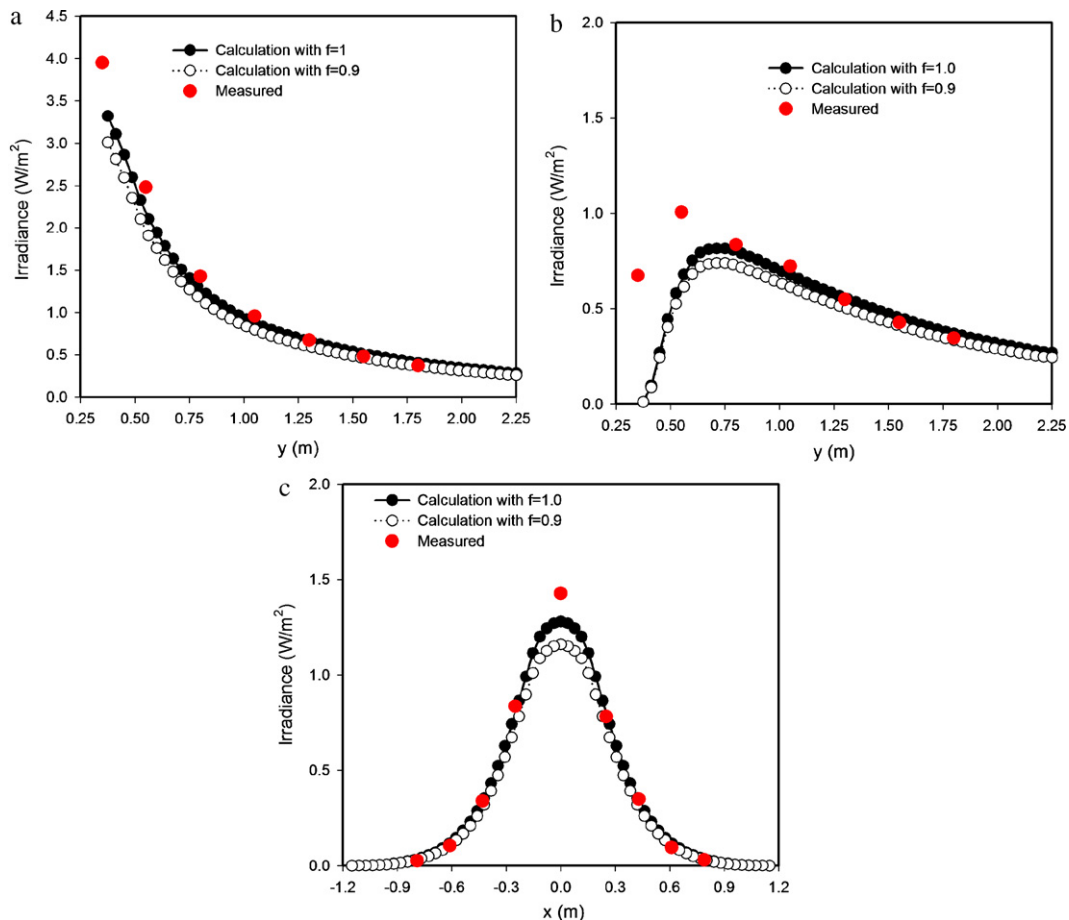

Fig. 14. Results of different reflectance of reflector with $f(x) = 1.0$ at $z = 2.05$ m: (a) E–E, (b) D–D and (c) A–A.
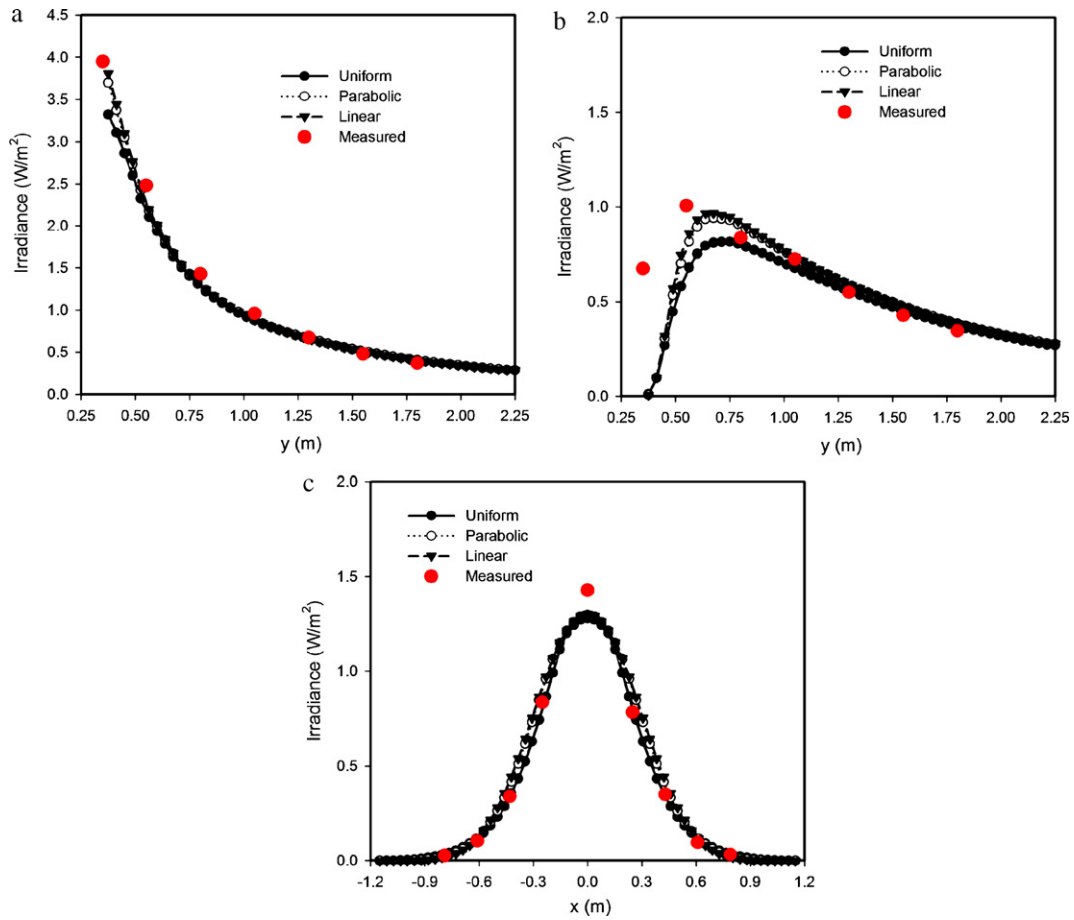
Fig. 15. Results of different irradiative source intensity distribution methods with f = 1.0 at z = 2.05 m: (a) E–E, (b) D–D and (c) A–A.

Table 2
Function for irradiative source intensity distribution methods.

$f(x)$	Uniform	Parabolic	Linear
$-(L_s/2) \leq x \leq (L_s/2)$	1.0	$-(6/L_s^2)x^2 + (3/2)$	$-(4/L_s)|x| + 2$

bution methods are shown in Fig. 15. Inferring from the results, parabolic and linear distribution give similar irradiance field and these results agree slightly better with the measurements than those by uniform distribution. We can conclude that uniform distribution function gives acceptable results for most engineering applications. Otherwise, the parameters (f or $f(x)$) of the model can be tailor-adjusted to fit the specific conditions.

5. Conclusions

In this work, we developed a novel mathematical model to evaluate UV irradiance intensity for indoor upper-room UVGI systems. The model is simple to apply yet high accuracy results can be obtained. By introducing a fictitious irradiation surface near the louver slots, the view factor approach is applied to compute the UV irradiance in a three-dimensional space with accounting for the influence from the louvers. This approach eliminates applying complex geometries for modeling physical boundaries and features of UVGI systems. The model was validated through comprehensive comparisons to experimental measurements, which were performed in a full-scale environmental controlled chamber, in which one UVGI fixture was mounted on a sidewall. The UV intensity distribution predicted by the present model agrees very well with the experimental measurements. This model has great poten-

tial for optimizing the design of indoor upper-room UVGI systems. The effects on the accuracy of the model were also discussed.

Acknowledgement

Appendix A. The algebraic operation of UV view factor

Considering from Eqs. (6) and (7), the view factor algebraic formula for indoor spatial viewpoint can be categorized into four cases. The dimensions of the finite visible surfaces for each case are shown in Fig. A1.

Case 1 ($W_2 < 0$, $W_3 < 0$): If P falls into region I for both the $\mathbf{n}_2$ and $\mathbf{n}_3$ directions, as shown in Fig. A1(a), the sub-surface of the louver slot is divided into 4 valid finite surfaces (QBRP′, RCSP′, TAQP′, and SDTP′) with their common corners aligned to the differential area at the Point P′, the projection of P on the sub-surface. In this case, the view factor between the differential area and the sub-surface of slot i is,

$$F_{d1-i} = \sum_{f=1}^{4} F_{d1-f} \qquad (A.1)$$

Case 2 ($W_2 > 0$, $W_3 < 0$): If P falls into the side of region I for both the $\mathbf{n}_2$ and $\mathbf{n}_3$ directions, as shown in Fig. A1(b), by introducing some ghost surfaces (QBSP′, PSCF′, QREP′, P′ETF), the view factor

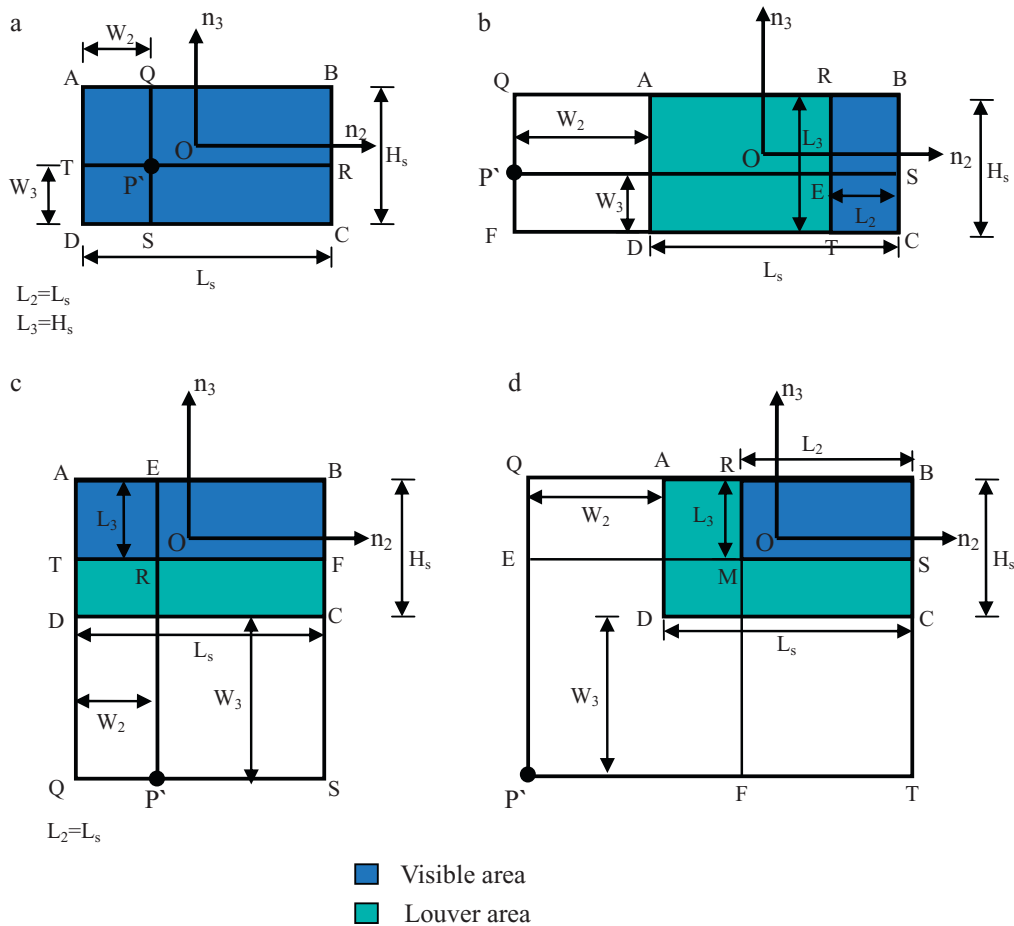**Fig. A1.** The view factor area with different cases when view point location projects on the plane of the louver: (a) Case 1 ($W_2 < 0$, $W_3 < 0$); (b) Case 2 ($W_2 > 0$, $W_3 < 0$); (c) Case 3 ($W_2 < 0$, $W_3 > 0$); (d) Case 4 ($W_2 > 0$, $W_3 > 0$).

Table A1
Dimensions of the four finite surfaces when P falls into different locations.

	Surface 1	Surface 2	Surface 3	Surface 4
a	$W_3 + H_s$	$\|W_3 + H_s - L_3\|$	$W_3 + H_s$	$\|W_3 + H_s - L_3\|$
b	$W_2 + L_s$	$W_2 + L_s$	$\|W_2 + L_s - L_2\|$	$\|W_2 + L_s - L_2\|$

can be calculated as

$$F_{d1-i} = F_{d1-1} + F_{d1-2} - F_{d1-3} - F_{d1-4} \qquad (A.2)$$

Case 3 ($W_2 < 0$, $W_3 > 0$): If P falls into the down of region I for both the $\mathbf{n}_2$ and $\mathbf{n}_3$ directions, as shown in Fig. A1(c), by introducing some ghost surfaces (P′EBS, P′RFS, QAEP′, QTRP′), the view factor can be calculated as

$$F_{d1-i} = F_{d1-1} - F_{d1-2} + F_{d1-3} - F_{d1-4} \qquad (A.3)$$

Case 4 ($W_2 > 0$, $W_3 > 0$): If P falls into region II for both the $\mathbf{n}_2$ and $\mathbf{n}_3$ directions, as shown in Fig. A1(d), by introducing some ghost surfaces (QBTP′, ESTP′, QRFP′, and EMFP), the view factor can be calculated as

$$F_{d1-i} = F_{d1-1} + F_{d1-2} - F_{d1-3} - F_{d1-4} \qquad (A.4)$$

In the above cases, the width and length of the four finite surfaces are listed in Table A1 and the normal distance is $c = W_1$.

References

[1] P. Fabian, J. McDevitt, W. DeHaan, R. Fung, B. Cowling, K. Chan, G. Leung, D. Milton, Influenza virus in human exhaled breath: an observational study, PLoS One 3 (2008) e2691.

[2] C.B. Beggs, The airborne transmission of infection in hospital buildings: fact or fiction? Indoor Built Environ. 12 (2003) 9–18.

[3] N. Lee, A. Wu, P. Chan, P. Cameron, G.M. Joynt, A. Ahuja, M.Y. Yung, C.B. Leung, K.F. To, S.F. Lui, C.C. Szeto, S. Chung, J.J.Y. Sung, A major outbreak of severe acute respiratory syndrome in Hong Kong, N. Engl. J. Med. 348 (2003) 1986–1994.

[4] F.S. Dawood, S. Jain, L. Finelli, M.W. Shaw, S. Lindstrom, R.J. Garten, L.V. Gubareva, X.Y. Xu, C.B. Bridges, T.M. Uyeki, Emergence of a novel swine-origin influenza A (H1N1) virus in humans novel swine-origin influenza (H1N1) virus investigation team, N. Engl. J. Med. 360 (2009) 2605–2615.

[5] S. Stelzer-Braid, B.G. Oliver, A.J. Blazey, E. Argent, T.P. Newsome, W.D. Rawlinson, E.R. Tovey, Exhalation of respiratory viruses by breathing, coughing and talking, J. Med. Virol. 81 (2009) 1674–1679.

[6] C.Y.H. Chao, M.P. Wan, L. Morawska, G.R. Johnson, Z.D. Ristovski, M. Hargreaves, K. Mengersen, S. Corbett, Y. Li, X. Xie, D. Katoshevski, Characterization of expiration air jets and droplet size distributions immediately at the mouth opening, J. Aerosol Sci. 40 (2009) 122–133.

[7] W.F. Wells, M.W. Wells, Measurement of sanitary ventilation, Am. J. Public Health 28 (1938) 343–350.

[8] W.F. Wells, M.W. Wells, T.S. Wilder, The environmental control of epidemic contagion. I. An epidemiological study of radiant disinfection of air in day schools, Am. J. Hyg. 35 (1942) 97–121.

[9] R.L. Riley, M. Knight, G. Middlebrook, Ultraviolet susceptibility of BCG and virulent Tubercle Bacilli, Am. Rev. Respir. Dis. 113 (1976) 413–418.

[10] R.L. Riley, E.A. Nardell, Clearing the air: the theory and application of ultraviolet air disinfection, Am. Rev. Respir. Dis. 139 (1989) 1286–1294.

[11] CDC, Guidelines for Preventing the Transmission of Mycobacterium tuberculosis in Health-Care Settings, Centers for Diseases Control and Prevention, Morbidity and Mortality Weekly Report, CDC, MMWR 54 (No. RR-17), 2005.

[12] E.A. Nardell, S.J. Bucher, P.W. Brickner, C. Wang, R.L. Vincent, K. Becan-McBride, M.A. James, M. Michale, J.D. Wright, Safety of upper-room ultraviolet germicidal air disinfection for room occupants: results from tuberculosis ultraviolet shelter study, Public Health Rep. 123 (2008) 52–60.

[13] ACGIH, Threshold Limit Values for Chemical Substances and Physical Agents: Biological Exposure Indices, Cincinnati, Ohio, American Conference of Governmental Industrial Hygienists, 2004.

[14] C.B. Beggs, K.G. Kerr, J.K. Donnelly, P.A. Sleigh, D.D. Mara, G. Cairns, An engineering approach to the control of Mycobacterium tuberculosis and other airborne

pathogens: a UK hospital based pilot study, Trans. Roy. Soc. Trop. Med. Hyg. 94 (2000) 141–146.

[15] G. Ko, M.W. First, H.A. Burge, The characterization of upper-room ultraviolet germicidal irradiation in inactivating airborne microorganisms, Environ. Health Perspect. 110 (2002) 95–101.

[16] P. Xu, E. Kujundzic, J. Peccia, M. Schafer, G. Moss, M. Hernandez, S.L. Miller, Impact of environmental factors on efficacy of upper-room air ultraviolet irradiation for inactivating airborne Mycobacteria, Environ. Sci. Technol. 39 (2005) 9656–9664.

[17] S.L. Miller, M.J. Macher, Evaluation of a methodology for quantifying the effect of room air ultraviolet germicidal irradiation on airborne bacteria, Aerosol Sci. Technol. 33 (2000) 274–295.

[18] P. Xu, J. Peccia, P. Fabian, J.W. Martyny, K.P. Fennelly, M. Hernandez, S.L. Miller, Efficacy of ultraviolet germicidal irradiation of upper-room air inactivating airborne bacterial spores and mycobacteria in full-scale studies, Atmos. Environ. 37 (2003) 405–419.

[19] C.J. Noakes, P.A. Sleigh, L.A. Fletcher, C.B. Beggs, Use of CFD modeling to optimise the design of upper-room UVGI disinfection systems for ventilated rooms, Indoor Built Environ. 15 (2006) 347–356.

[20] M. Sung, S. Kato, Method to evaluate UV dose of upper-room UVGI system using the concept of ventilation efficiency, Build. Environ. 45 (2010) 1626–1631.

[21] M.W. First, E.A. Nardell, W. Chaisson, R. Riley, Guidelines for the application of upper-room ultraviolet germicidal irradiation for preventing transmission of airborne contagion. Part I. Basic principles, ASHRAE Trans. 105 (Pt 1) (1999) 869–876, CH-99-12-1.

[22] M.W. First, E.A. Nardell, W. Chaisson, R. Riley, Guidelines for the application of upper-room ultraviolet germicidal irradiation for preventing transmission of airborne contagion. Part II. Design and operation guidance, ASHRAE Trans. 105 (1999) 877–887, CH-99-12-2.

[23] R.L. Riley, S. Permutt, Room air disinfection by ultraviolet irradiation of upper air: air mixing and germicidal effectiveness, Arch. Environ. Occup. Health 22 (1971) 208–219.

[24] C.B. Beggs, P.A. Sleigh, A quantitative method for evaluating the germicidal effect of upper room UV fields, J. Aerosol Sci. 33 (2002) 1681–1699.

[25] S.N. Rudnick, M.W. First, Fundamental factors affecting upper-room ultraviolet germicidal irradiation. Part II. Predicting effectiveness, J. Occup. Environ. Hyg. 4 (2007) 352–362.

[26] M. Nicas, S.L. Miller, A multi-zone model evaluation of the efficacy of upper-room air ultraviolet germicidal irradiation, J. Occup. Environ. Hyg. 14 (1999) 317–328.

[27] C.J. Noakes, C.B. Beggs, P.A. Sleigh, Modeling the performance of upper room ultraviolet germicidal irradiation devices in ventilated rooms: comparison of analytical and CFD methods, Indoor Built Environ. 13 (2004) 477–488.

[28] C.J. Noakes, L.A. Fletcher, C.B. Beggs, P.A. Sleigh, K.G. Kerr, Development of a numerical model to simulate the biological inactivation of airborne microorganisms in the presence of ultraviolet light, J. Aerosol Sci. 35 (2004) 489–507.

[29] W. Kowalski, W. Bahnfleth, Effective UVGI system design through improved modeling, ASHRAE Trans. 106 (Pt 2) (2000) 721–730, MN-00-11-1.

[30] W.J. Kowalski, W.P. Bahnfleth, D.L. Witham, B.F. Severin, T.S. Whittam, Mathematical modeling of ultraviolet germicidal irradiation for air disinfection, Quant. Microbiol. 2 (2000) 249–270.

[31] L.F. Zhang, W.A. Anderson, A finite model for the prediction of the UV radiation field around a linear lamp, Chem. Eng. Sci. 65 (2010) 1513–1521.

[32] S.N. Rudnick, Predicting the ultraviolet radiation distribution in a room with multilouvered germicidal fixtures, AIHAJ 62 (2001) 434–445.

[33] M.F. Modest, Radiative Heat Transfer, second ed., McGraw-Hill, New York, 1993.

[34] R.O. Rahn, P. Xu, S.L. Miller, Dosimetry of room-air germicidal (254 nm) radiation using spherical actinometry, Photochem. Photobiol. 70 (1999) 314–318.

[35] S. Jin, K.G. Linden, J. Ducoste, D. Liu, Impact of lamp shadowing and reflection on the fluence rate distribution in a multiple low-pressure UV lamp array, Water Res. 39 (2005) 2711–2721.

[36] W. Kowalski, Ultraviolet Germicidal Irradiation Handbook, first ed., Springer, New York, 2009.

[37] W.B. Elmer, The Optical Design of Reflectors, second ed., John Wiley & Sons, New York, 1980.